ACS OMEGA

Open Access

http://pubs.acs.org/journal/acsodf

Article

Exploring a Low-Cost Valorization Route for Amazonian Cocoa Pod Husks through Thermochemical and Catalytic Upgrading of Pyrolysis Vapors

Yanet Villasana,* Sabino Armenise, Javier Ábrego, María Atienza-Martínez, Karina Hablich, Fernando Bimbela, Alfonso Cornejo, and Luis M. Gandía

Cite This: *ACS Omega* 2023, 8, 37610−37621

Read Online

ACCESS | Metrics & More | Article Recommendations | Supporting Information

ABSTRACT: Ecuador as an international leader in the production of cocoa beans produced more than 300 000 tons in 2021; hence, the management and valorization of the 2 MM tons of waste generated annually by this industry have a strategic and socioeconomic value. Consequently, appropriate technologies to avoid environmental problems and promote sustainable development and the bioeconomy, especially considering that this is a megadiverse country, are of the utmost relevance. For this reason, we explored a low-cost pyrolysis route for valorizing cocoa pod husks from Ecuador's Amazonian region, aiming at producing pyrolysis liquids (bio-oil), biochar, and gas as an alternative chemical source from cocoa residues in the absence of hydrogen. Downstream catalytic processing of hot pyrolysis vapors using Mo- and/or Ni-based catalysts and standalone γ-Al_2O_3 was applied for obtaining upgraded bio-oils in a laboratory-scale fixed bed reactor, at 500 °C in a N_2 atmosphere. As a result, bimetallic catalysts increased the bio-oil aqueous phase yield by 6.6%, at the expense of the organic phase due to cracking reactions according to nuclear magnetic resonance (NMR) and gas chromatography−mass spectrometry (GC−MS) results. Overall product yield remained constant, in comparison to pyrolysis without any downstream catalytic treatment (bio-oil ∼39.0−40.0 wt % and permanent gases 24.6−26.6 wt %). Ex situ reduced and passivated MoNi/γ-Al_2O_3 led to the lowest organic phase and highest aqueous phase yields. The product distribution between the two liquid phases was also modified by the catalytic upgrading experiments carried out, according to heteronuclear single-quantum correlation (HSQC), total correlation spectroscopy (TOCSY), and NMR analyses. The detailed composition distribution reported here shows the chemical production potential of this residue and serves as a starting point for subsequent valorizing technologies and/or processes in the food and nonfood industry beneficiating society, environment, economy, and research.

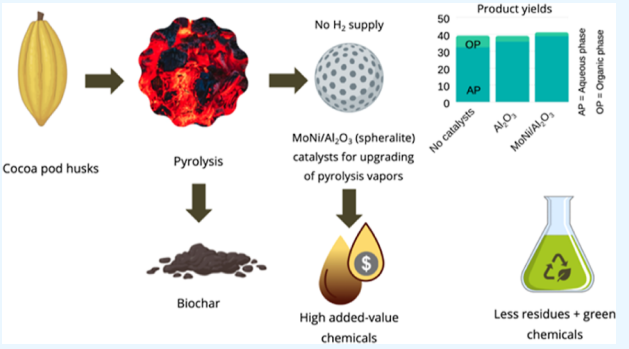

1. INTRODUCTION

Ecuador is a major world trader of cocoa beans, producing 365 thousand tons in 2021, representing an export value of $700 million, ranking seventh in the world. However, each year 2 MM tons of residues remain in the field, risking environmental health, especially when producing in the Amazon region, instead of being transformed into an alternative chemicals source.[1−3] In this context, biorefinery strategies could be adopted for the valorization of these wastes while protecting the megadiversity of this country. Thermochemical routes such as pyrolysis can be used for producing bio-oil, biochar, and combustible gas from cocoa pod husks, which are composed of hemicellulose, cellulose, lignin, pectin, and crude fiber.[4]

Biomass pyrolysis liquids (usually named as bio-oil) can be regarded as a valuable intermediate that may be used as starting raw material for obtaining several value-added chemicals.[5−13] Indeed, some biobased products derived from biomass pyrolysis liquids have successfully reached commercialization in the market.[5,8,11,14,15] However, the direct use of bio-oil as biofuel in transportation is still hampered and not viable to date owing to the significant differences in its fuel properties compared to drop-in fuels derived from fossil resources. In fact, because of their nature and their characteristic physicochemical properties, namely, its low chemical stability, low heating value and high corrosiveness, the as-produced bio-oils cannot meet the present standards imposed onto fuels, which are related to the high oxygen content in bio-oil compared to fossil-derived fuels.[15,16] Hydroprocessing

Received: September 4, 2023
Accepted: September 18, 2023
Published: September 28, 2023

routes have been widely investigated as a strategy to enhance bio-oil quality and excellent reviews can be found in the literature,[16−19] usually requiring the availability of hydrogen and high pressure.[20] One option is the catalytic upgrading of biomass hot pyrolysis vapors before collecting bio-oils using different proofs of concept and catalytic formulations. As recently reviewed by Seshan's group,[21] the ex situ downstream catalytic conversion of biomass pyrolysis vapors has been deemed effective and practical for enhancing bio-oil quality. Regarding the choice of catalyst, upgrading of pyrolysis vapors both in situ and ex situ using zeolites, mainly ZSM-5,[22] β, and Y zeolites[23] has been widely researched, benefiting from previous vast experience in upgrading of hydrocarbons in the oil industry. Other aluminosilicates and mesoporous materials including alkaline and alkaline-earth metal-based catalysts applications have been reported.[21,24−26] Furthermore, metal oxides of Ti, Sn, Zr, Ce, and Mo are effective in deoxygenation of biomass pyrolysis vapors because of their acid and reducible metal sites.[27] Unsupported nickel oxide (NiO) was tested for the downstream upgrading of pyrolysis vapors from beech wood.[28] Consequently, the authors concluded that NiO was the most selective catalyst toward oxygen removal by CO_2 production and regarded it as an interesting candidate for its incorporation in other support materials and evaluation of the derived Ni-based catalysts in biomass pyrolysis.

Some of these metals, such as Ce and Mo, count on oxygen vacancy sites that can easily facilitate O transfer by the existence of easily reducible redox pairs, thereby promoting O adsorption and deoxygenation reactions.[29] In addition, by acting as O reservoirs they can eliminate carbon deposits from the catalyst surface, therefore alleviating deactivation,[13] the main setback for these technologies at larger scales. Particularly, Mo have been widely studied as active phase in catalysts for hydrotreating of biomass pyrolysis liquids, often in bimetallic sulfided NiMo formulations, derived from commercial hydrodesulfurization catalysts used in the crude-oil refinery industry.[19] Bimetallic NiMo and CoMo commercial hydrotreating catalysts have been mostly applied in hydrotreatment of pyrolysis liquids obtained from different biomass sources,[30] with some successful results in the complete removal of N heteroatoms from sewage sludge bio-oils in batch hydrotreatment using H_2.[31] Various biomass-derived pyrolysis liquids have been treated using NiMo catalysts including rapeseed, poplar wood, white oak, and poplar sawdust;[32] more recently, wheat straw bio-oils were also upgraded.[33]

As concerns catalytic upgrading of biomass pyrolysis vapors using Mo-based catalysts, studies are still scarce. Most of the literature focuses on upgrading tests at microscale setups and/or using single model compounds, as *m*-cresol,[34] anisole,[35] or phenol.[36] In these studies, the catalyst conducts effective HDO while attaining high conversion levels and resistance toward deactivation by C deposition and coke formation. Murugappan et al.[37] tested a 10 wt % MoO_3 catalyst supported on TiO_2 and ZrO_2 in the upgrading of pine pyrolysis vapors and found that low biomass-to-MoO_3 mass ratios yielded predominantly olefinic and aromatic hydrocarbons, while greater values of that ratio resulted in a decrease of olefins and aromatics and the presence of partially deoxygenated species (mostly furans and phenols). Zhou et al.[38] also analyzed MoO_3 but in the downstream upgrading of pyrolysis vapors of beech wood, leading to cracking reactions above 450 °C yielding more gaseous species instead of HDO forming hydrocarbons. Moreover, a previous report of Kukushkin et al. suggested that a higher content of Mo in the Ni−Cu−Mo/Al_2O_3 catalysts (from 0.0 to 6.9%) leads to an increase in the yield of normal alkanes during esters HDO.[39]

Downstream catalytic upgrading treatments promote a better contact between the catalyst and the pyrolysis vapors, where deoxygenation by metal oxides can be notably enhanced by cofeeding H_2 in the process. This is quite appealing in the present scenario of power-to-gas concepts established in developed countries, boosted in recent years by significant advances in high-purity H_2 production by water electrolysis along with solar photovoltaic and wind farms. However, in the context of isolated and socio-economically depressed areas, where access to advanced processing technologies and costly commodities such as high-pressure hydrogen may be virtually impossible, simple, low-cost, and effective strategies for valorization of residual biomass must be favored. Using inexpensive bulk or low-cost catalysts and simple concept proofs for producing upgraded bio-oil from agricultural wastes could have a beneficial impact on the economic activity of such communities, while developing a biobased economy that could produce renewable fuels and other commodities. In spite of being a low-cost material with potentially interesting properties, some studies have ruled out γ-Al_2O_3 as an adequate catalyst support for effectively upgrading pyrolysis vapors,[40,41] even though additional research should be carried out to elucidate the role of catalyst supports in deoxygenation, as discussed by Rogers and Zheng.[42]

As stated in recent literature reviews,[20] there is scarcity of works on the catalytic upgrading of real biomass vapors at scales large enough to provide relevant insights for further scaling-up of the proposed technologies. Clearly, this gap must be addressed. There are not many works on pyrolysis of cocoa pod husks, and even less on the further catalytic treatment of their pyrolysis vapors, available in the published literature, as far as we know.

For these reasons, the present work aims at characterizing the products obtained in the pyrolysis of Amazonian cocoa pod husks combined with downstream catalytic upgrading of pyrolysis hot vapors using bare alumina (γ-Al_2O_3), and Ni, Mo, and MoNi catalysts supported on it as well with a high content of Mo (7:1). This paper discloses the possibility to improve the liquids products without using external H_2 source, which has been recently reported.[43] Both metal active phases have been widely used in different catalyst formulations for refinery hydrotreating processes focused on removing heteroatoms from the hydrocarbon pool of certain crude-oil cuts, showing adequate activity for hydrogenolysis reactions while displaying moderate activity in the undesired hydrogenation of aromatic compounds.[44] A two-stage fixed bed catalytic upgrading setup, consisting of a fixed bed pyrolyzer and a catalytic fixed bed placed downstream, was used to analyze the changes in the product distribution and the bio-oil properties after the catalytic treatment of pyrolysis hot vapors under a hydrogen-free atmosphere.

2. MATERIALS AND METHODS

2.1. Amazonian Cocoa Pod Husks. Amazonian cocoa pod husks were obtained from local producers in Tena, Ecuador. Samples were cut in chips of approximately 1 cm diameter and dried at 105 °C until a constant weight was achieved before pyrolytic reactions. Proximate analysis was performed following ISO-589-1981, ISO-18122-2015, and ISO-5623-1974 standards for moisture, ash, and volatiles

https://doi.org/10.1021/acsomega.3c06672
ACS Omega 2023, 8, 37610−37621

content, respectively (fixed carbon was calculated by difference). Ultimate analysis was performed using a Leco TruSpec Micro elemental analyzer. The higher heating value (HHV) was determined using a C2000 basic calorimeter by IKA (Table 1).

Table 1. Properties of the Amazonian Cocoa Pod Husks Used (as Received)

	analytical standard	Amazonian cocoa pod husks
dry matter (wt %)	ISO 18134-2:2017	92.6
ash (wt %)	ISO 18122:2016	8.8
volatiles (wt %)	ISO 18123:2016	74.2
fixed carbon (wt %)	[a]	9.6
carbon (wt %)	[b]	42.9
hydrogen (wt %)	[b]	5.7
nitrogen (wt %)	[b]	0.7
sulfur (wt %)	[b]	b.d.l[e]
oxygen (wt %)	[c]	41.9
HHV (MJ/kg)	[d]	16.7

[a]By difference. [b]Ultimate analysis was performed using Leco TruSpec Micro elemental analyzer. [c]Oxygen (wt %) = 100 − carbon (%) − hydrogen (%) − nitrogen (%) − sulfur (%) − ash (%). [d]Determined using C2000 basic calorimeter by IKA. [e]Below detection limits.

2.2. Preparation and Characterization of Catalysts. The catalysts used in this process were based on Ni and Mo monometallic (1 and 7 wt %, respectively) and bimetallic formulations to obtain a MoNi ratio of (7:1), which were deposited by a strong electrostatic adsorption method on a commercial γ-Al_2O_3 support (Spheralite 505, Axens Procatalyst Catalysts & Adsorbents) in the form of spherical pellets (particle size ~0.5 mm). Metals were deposited on the support (previously dried in an oven at 150 °C for 2 h) as described elsewhere.[45] Twenty-nine grams of $Ni(NO_3)_2{\cdot}6H_2O$ (pure, Sigma-Aldrich), 80 g of NH_4NO_3 (pure, Sigma-Aldrich), and 4 mL of ammonia solution (25%) were mixed and added to deionized water to obtain 1 L of pH-neutral 0.1 M solution of Ni. The same process was adapted to molybdenum deposition using $(NH_4)_6Mo_7O_{24}{\cdot}6H_2O$ (pure, Sigma-Aldrich) to obtain a 0.1 M solution. A MoNi bimetallic catalyst was prepared by successive impregnations and a calcination stage between them.

Spheralite pellets were immersed in each metallic solution for 24 h at room temperature with continuous stirring. After adsorption, catalysts were allowed to dry for 24 h at room temperature and calcined in an air flow (100 mL/min) at 350 °C for 3 h with a heating ramp of 2 °C/min. Prior to the catalytic tests, the supported metal catalysts were prereduced ex situ and passivated in a Microactivity XS15 automated reaction setup (Process Integral Development, PID Eng & Tech, Spain), which consisted of a tubular quartz reactor in a fixed bed configuration. The calcined precursors were heated to 500 °C following a 10 °C/min ramp in a N_2 flow (60 N cm^3/min). Next, the reduction of the solids was carried out at 500 °C for 3 h in a pure H_2 flow (100 N cm^3/min). Then, the reactor was cooled down to 20 °C in a N_2 flow (60 N cm^3/min), and afterward, the catalysts were readily subjected to passivation by exposing them to a diluted O_2 flow (0.5% O_2 in Ar, 25 N cm^3/min) during 45 min.

Catalysts were characterized by inductively coupled plasma-optical emission spectrometry (ICP-OES), N_2 adsorption, H_2 temperature-programmed reduction (TPR), CO chemisorption, and X-ray diffraction (XRD). In addition, some spent samples after reaction were characterized by temperature-programmed oxidation coupled to mass spectrometry (TPO-MS). Details of catalyst characterization are included in the Supporting Information.

2.3. Pyrolysis Experiments. *2.3.1. Pyrolysis.* Pyrolysis of Amazonian cocoa pod husks was carried out in a bench-scale pyrolysis system (Figure 1) that has been previously used for the pyrolysis of various wastes[46] with minor modifications, namely, the use of a fixed bed reactor with a smaller diameter, in order to minimize radial temperature gradients during pyrolysis. The system consists mainly of a cylindrical batch pyrolysis reactor with an inner diameter of 40 mm and a length of 200 mm. 100 g of cocoa pod husks were placed inside the reactor for each run. Three K-type thermocouples were placed at different positions to register the temperature profiles inside the reactor. The reactor temperature throughout the experiments was taken as an average of the three thermocouple readings, considering temperature differences at the final set

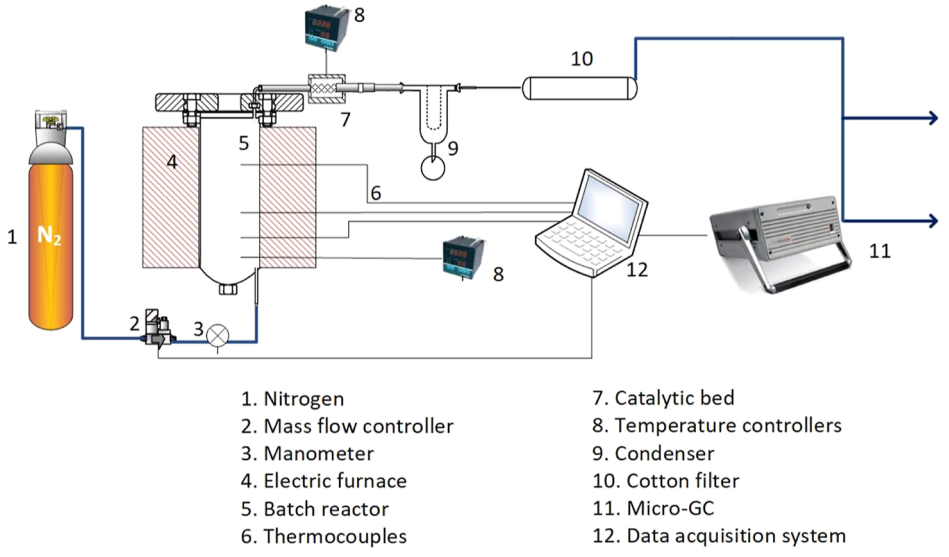

Figure 1. Scheme of the reaction system used for pyrolysis experiments. Authors confirm that this is an original image elaborated by one coauthor.

https://doi.org/10.1021/acsomega.3c06672
ACS Omega 2023, 8, 37610−37621

point lower than 20°. Experiments were performed at a final temperature of 500 °C at an approximate heating rate of 10 °C/min, and N_2 was used as the carrier gas (100 N cm^3/min, GHSV = 24 h^{-1}). The vapors produced during pyrolysis exited the reactor through an outlet in the upper side of the pyrolysis reactor.

Next, the condensable vapors (both water and organic compounds) were collected in the condensation system (two ice-cooled condensers and a cotton filter). The evolution of the permanent gaseous products (specifically, CO_2, CO, H_2, CH_4, C_2H_2, C_2H_4, C_2H_6, and H_2S) was monitored by gas chromatography (GC). The mass yields of solids (char) and bio-oil were determined gravimetrically. The mass yield of permanent gases was calculated by difference. Mass balance closure of this experimental system was reported to be higher than 90% for all the experiments performed.[46] The analytical uncertainty associated with the experimental data is considered less than 3% based on previous studies by the authors of this work in the same experimental setup and with similar materials.[46,47]

Amazonian cocoa pod husk composition and stability during thermal treatments were analyzed by thermogravimetric analysis (TGA) using a NETZSCH STA 449 Jupiter instrument. The sample (around 10 mg) was heated up to 500 °C at a heating rate of 10 °C/min in a N_2 atmosphere (150 N cm^3/min).

2.3.2. Pyrolysis Followed by Downstream Catalytic Upgrading of Hot Pyrolysis Vapors. The catalytic upgrading of hot pyrolysis vapors was carried out placing an additional bed of prereduced catalysts, which was placed in a downstream section separated from the pyrolytic zone. The cylindrical stainless-steel catalytic reactor has a fixed bed reactor configuration with the following dimensions: 35 mm inner diameter and 100 mm of length.

The temperature of the pyrolytic zone was 500 °C, while the temperature of the catalytic zone was 400 °C. Catalyst loading was 1.0 wt % referred to the amount of Amazonian cocoa pod husks loaded in the pyrolytic reactor. The catalytic bed density (including the interparticle void fraction) was 0.74 g/cm^3. As a result, typical spatial velocities $\leqslant$0.5 h^{-1} were set in the catalytic bed. Such low values were selected to ensure that a fresh catalyst could be available for upgrading the vapors throughout the whole duration of the experimental runs.

The effect of each metal was analyzed by comparison of the products distribution during pyrolysis in the presence of Ni, Mo, and MoNi catalysts. In addition, the possible catalytic effect of the γ-Al_2O_3 spheres used as support was also investigated by filling in the catalytic reaction zone with bare γ-Al_2O_3 pellets as the filler bed.

2.4. Bio-Oil Characterization. The as-obtained bio-oil in all of the experiments separated into two different phases, an organic phase (OP) and an aqueous phase (AP). The bio-oil was centrifuged to facilitate the collection and characterization of each phase. The water content of both phases was measured by Karl Fischer titration (Mettler Toledo V-20, titrant: Hydranal-composite 5K one-component in Hydranal-medium K). The elemental composition of the OP was analyzed (LECO TruSpec Micro) and the higher heating value (as-produced, HHV_{ap}) was calculated using the correlation proposed by Channiwala and Parikh[48] taking into account the water content. The chemical composition of both the OP and the AP was semiquantitatively analyzed using an Agilent 7890A gas chromatograph (GC)-flame ionization detector (FID) system coupled with an Agilent 5975C inert mass spectrometry detector (MS) and equipped with capillary columns of different polarities (Agilent DB-17 ms and Agilent HP-FFAP). Dichloromethane was used as solvent for the OP (more details are included in the Supporting Information).

Nuclear magnetic resonance (NMR) measurements were done at 300 K on a Bruker Ascend III spectrometer equipped with a PABBO 5 probe, at 400 and 101 MHz for ^1H and ^{13}C, respectively, and was processed using Topspin 3.2 software (more details in the Supporting Information).

3. RESULTS AND DISCUSSION

3.1. Characterization of the Fresh Catalysts. Ni and Mo incorporation in monometallic catalysts was quantitative. However, the low loading percentage of Ni indicates a poor incorporation in the bimetallic catalyst (Table 2), which confirmed the XRD and TPR results (Figures 2 and 3). The discrepancy found between the nominal and the real metal contents in the MoNi bimetallic catalyst could be related to the preparation method by electrostatic adsorption. This method has the advantage of yielding high metallic dispersions but at times it can result in an incomplete incorporation of the metals onto the support.[49]

Table 2. Metal Composition of Fresh Catalysts Was Determined by ICP-OES

catalysts	nominal		experimental	
	Mo (wt %)	Ni (wt %)	Mo (wt %)	Ni (wt %)
Mo/Al_2O_3	7		7.3	
Ni/Al_2O_3		1		0.9
$MoNi/Al_2O_3$	7	1	5.9	0.40

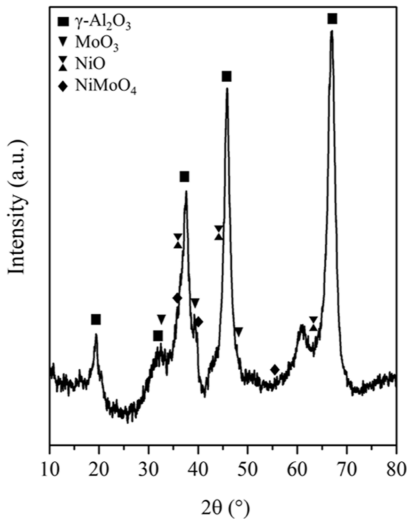

Figure 2. XRD pattern of fresh MoNi catalyst (prereduced and passivated).

The XRD pattern of the bimetallic catalyst showed signals attributable to crystalline Al_2O_3 from the alumina support and to oxide species of the corresponding metals used as active phases (Figure 2). In addition, signals suggesting the presence of a bimetallic phase identified as monoclinic primitive $NiMoO_4$ were subtly found. Nevertheless, peaks associated

https://doi.org/10.1021/acsomega.3c06672
ACS Omega 2023, 8, 37610−37621

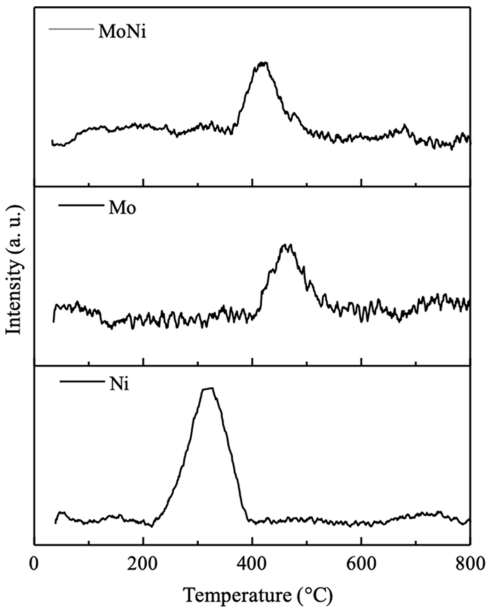

Figure 3. H_2-TPR profiles of the fresh catalysts.

with nickel structures were difficult to elucidate, likely due to the low loading of this metal in the catalyst (see the Supporting Information for details on structure identification and peaks assignment).

N_2 physisorption did not show any significant variation in the textural properties between catalysts (Table 3). As for the metallic surface area measured by CO chemisorption after in situ reduction of the samples, S_{AC}, relatively low metal surface areas were obtained in all cases, probably due to the formation of Ni and Mo alloys with the γ-Al_2O_3 support or by effects related to strong metal support interaction, which is inferred by the results recorded by TPR (Table 3) (see also Supporting Information for details in catalyst reduction and chemisorption analysis and textural properties, respectively). The monometallic Ni catalyst shows 3−4-fold smaller particles than molybdenum or bimetallic ones, which is in agreement with the better metal dispersion shown by this catalyst, as previously reported.[50] H_2-TPR profiles revealed interactions between Mo and Ni with the alumina support in the catalysts (Figure 3). For Ni/γ-Al_2O_3, the maximum reduction temperature was shown as a broad band centered between 200 and 400 °C. For Mo/Al_2O_3, two main peaks were obtained, one at around 400−500 °C (maximum at around 450 °C) and another one at temperatures above 750 °C. The low-temperature peak has been assigned to the partial reduction ($Mo^{6+} \rightarrow Mo^{4+}$) of amorphous Mo oxides or heteropolymolybdates (octahedral Mo species) as reported earlier,[51,52] whereas the latter could be attributed to the partial reduction of amorphous tetrahedral polymolybdate MoO_3 species having a strong interaction with the support.[53] The TPR profile of MoNi/γ-Al_2O_3 also showed two main distinct reduction events: a low intensity reduction event peaking at around 300 °C and a major reduction peak with a maximum at 430 °C. The former could be attributed to the reduction of Ni species, and the low intensity found could be due to the low content of Ni in this catalyst, as evidenced by ICP-OES. The latter peak could be ascribed to the reduction of the Mo species. The peak temperature (430 °C) is lower than that found for the major reduction peak of the monometallic Mo catalyst (see discussion above), indicating that the addition of Ni promoted the reducibility of Mo (by decreasing its reduction temperature).[54]

3.2. Pyrolysis and Pyrolysis Followed by Downstream Catalytic Treatment of the Hot Vapors. *3.2.1. Products Distribution.* The thermogravimetric analysis (TGA) curve of Amazonian cocoa pod husks and its first derivative (DTG) results confirmed that this waste is suitable for pyrolysis processes due to its relatively easy thermal decomposition [Figure S3 (Supporting Information) along with a detailed discussion].

Table 4 gathers the product distribution from both Amazonian cocoa pod husk pyrolysis and pyrolysis, followed by downstream catalytic treatment of the hot vapors. The product distribution obtained was quite different to that reported by Adjin-Tetteh et al.,[4] especially in terms of yields of bio-oil and permanent gases, probably due to the different volatiles content in both cocoa pod husks used and to the different pyrolysis temperatures tested. As expected, the yield of char (33.8−34.8 wt %) did not vary because of the catalytic treatment, since this treatment was performed downstream from the pyrolysis reactor. The standard deviation of the char yields obtained is 34.5 ± 0.4, which is low and confirms that catalytic experiments were made under equivalent conditions in terms of liquid and gas inlet flows. Furthermore, the yields of both bio-oil (39.0−41.0 wt %) and permanent gases (24.6−26.6 wt %) remain constant regardless of the catalyst used and the reduction and passivation treatments performed. Bio-oil separated into two phases: an organic phase (OP) and an aqueous phase (AO) in all cases. Although the catalytic

Table 4. Product Distribution from Noncatalytic and Ex Situ Catalytic Pyrolysis of Amazonian Cocoa Pod Husks

catalyst	yield (wt %)				
	char	liquid product	OP	AP	gas[d]
none[a]	34.3	39.1	6.9	32.2	26.6
γ-Al_2O_3	34.8	39.0	3.4	35.6	26.2
Ni/γ-Al_2O_3 RP[c]	34.6	40.6	3.1	37.5	24.8
Mo/γ-Al_2O_3 RP[c]	34.6	40.8	4.8	36.0	24.6
MoNi/γ-Al_2O_3 UR[b]	34.8	40.3	6.3	34.0	24.9
MoNi/γ-Al_2O_3 RP[c]	33.8	41.0	2.2	38.8	25.2

[a]Standalone pyrolysis. [b]UR: unreduced catalyst. [c]RP: reduced and passivated catalyst. [d]By difference.

Table 3. Textural Properties of the Fresh Catalysts

catalysts	N_2-physisorption			CO-chemisorption		
	S_{BET}[a] (m^2/g)	V_p[b] (cm^3/g)	D_p[c] (Å)	active surface area, S_{AC} (m^2/g metal)	active particle diameter (nm)	dispersion (%)
Mo/γ-Al_2O_3	237	0.39	65	6.94 (0.51[d])	84.73	1.51
Ni/γ-Al_2O_3	249	0.43	66	27.26 (0.25[d])	24.72	4.09
MoNi/γ-Al_2O_3	248	0.40	63	9.44 (0.59[d])	63.00	2.00

[a]BET surface area. [b]Pore volume. [c]Pore diameter. [d]Active surface area calculated as m^2/g catalyst.

https://doi.org/10.1021/acsomega.3c06672
ACS Omega 2023, 8, 37610−37621

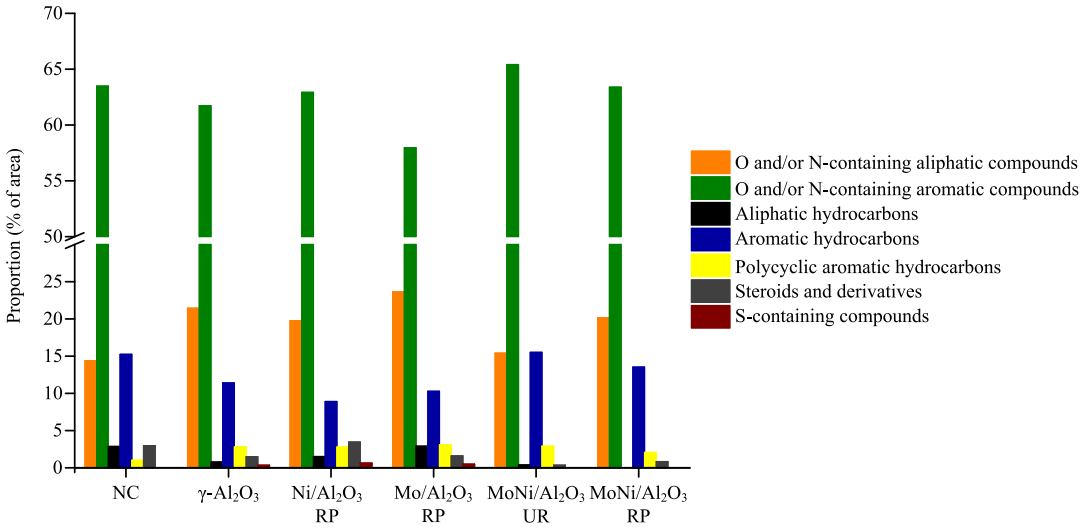

Figure 4. Composition of the OP obtained from standalone pyrolysis and from the downstream catalytic treatment of pyrolysis vapors of Amazonian cocoa pod husks.

Table 5. Physicochemical Characterization of the Liquid Product Obtained from Noncatalytic and Ex Situ Catalytic Pyrolysis of Amazonian Cocoa Pod Husks

catalyst	water content (wt %)		OP				
	OP	AP	C (%)	H (%)	N (%)	O (%)	HHV_{ap}[d] (MJ/kg)
none[a]	4.1	91.7	66.8	8.5	2.9	21.8	30.7
γ-Al_2O_3	4.9	84.7	68.6	8.3	2.5	20.6	31.2
Ni/γ-Al_2O_3 RP[c]	5.4	86.0	71.0	8.3	2.7	18.1	32.3
Mo/γ-Al_2O_3 RP[c]	4.0	84.5	68.0	8.3	2.5	21.1	31.1
MoNi/γ-Al_2O_3 UR[b]	5.0	86.0	70.5	8.4	2.8	18.3	32.3
MoNi/γ-Al_2O_3 RP[c]	5.6	85.2	64.2	7.9	3.0	25.0	28.7

[a]Standalone pyrolysis. [b]UR: unreduced catalysts. [c]RP: reduced and passivated catalyst. [d]HHV_{ap}: higher heating value as produced.

treatment did not have a significant effect on the total yield of bio-oil, it generally decreased the yield of the OP while increasing the yield of the AP. The MoNi/γ-Al_2O_3-RP catalyst led to the lowest OP and the highest AP yields. Therefore, it can be concluded that catalytic post-treatment of the hot pyrolysis vapors does not modify the overall yield to liquid product, but it can alter the relative distribution of products between the OP and the AP as well as the yield to these phases, which is in agreement with previous studies.[41,45]

3.2.2. Liquid Product Properties. The water content of the OP obtained by pyrolysis was 4.1 wt %. After the treatment of the pyrolysis hot vapors with different catalysts, the water content of the OP varied between 4.0 and 5.6 wt %. Thus, the catalytic treatment had little impact on this property. All the OP fractions showed C and O contents between 64.2 and 71.0 and 18.1−21.8 wt %, respectively, which in turn led to HHV_{ap} between 28.7 and 32.3 MJ/kg. Therefore, the use of downstream catalysts did not have a great effect on the calorific value of the OP obtained.

For the sake of clarity, the organic compounds identified in the OP by GC−MS have been grouped into the chemical families depicted in Figure 4. The OP was rich in phenol and its derivatives, and in ketones and toluene and its derivatives. Catalytic post-treatment affected the relative proportion of these. Oxygen and/or nitrogen-containing aromatic compounds were the most abundant organic compounds in the OP (chromatographic area percentage between 57 and 64%), followed by oxygen- and/or nitrogen-containing aliphatic compounds (chromatographic area of 14−22%) and aromatic hydrocarbons (chromatographic area of 9−16%).

In addition to decreasing the yield of OP, the catalytic treatment of the hot pyrolysis vapors had a slight effect on its composition. As concerns the different materials tested for the treatment of the hot pyrolysis vapors, it can be generally concluded that all the materials tested, except for MoNi/Al_2O_3 UR, altered the composition of the OP. The proportion of oxygen and/or nitrogen-containing aliphatic compounds was increased, while the aromatic hydrocarbons proportion decreased in comparison to the pyrolysis runs, probably due to catalyzed ring-opening reactions.[42] The use of standalone alumina as a catalytic bed did provide very similar results to those obtained using the monometallic Ni catalyst. Both materials increased the proportion of O- and/or N-containing aliphatic compounds in the OP from ∼14% in the NC run to ∼20% at the expense of the decrease in aromatics content from ∼16 to ∼10%. These results confirm that the use of alumina as inexpensive bulk material for preliminary catalytic upgrading of pyrolysis vapors poses an interesting strategy,[41] which could increase the effectiveness and time-on-stream of highly active and selective upgrading catalysts placed downstream from the pyrolysis unit.

Similar trends were observed in the case of the monometallic Mo catalyst, though this material also notably affected the content in the aromatic compounds of O and/or N, which had barely remained unaltered in the other catalytic treatments. In turn, the content in O and/or N-containing aliphatic

https://doi.org/10.1021/acsomega.3c06672
ACS Omega 2023, 8, 37610−37621

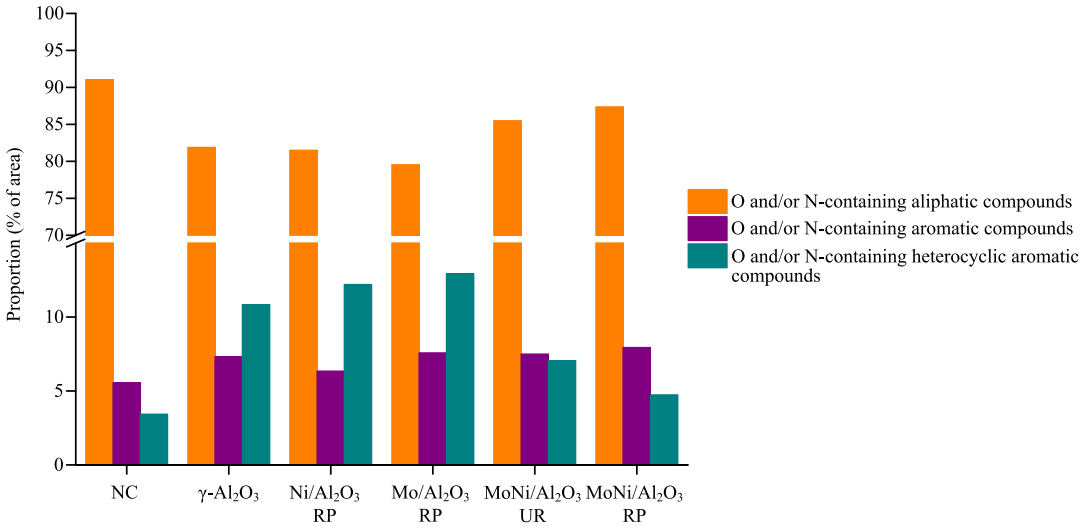

Figure 5. Composition of the AP obtained from stand-alone pyrolysis and from downstream catalytic treatment of pyrolysis vapors of Amazonian cocoa pod husks.

compounds was the highest. This increment in the content of aliphatic hydrocarbons at the expense of aromatic compounds displayed by the Mo catalyst can be explained by the notable hydrocracking activity of MoO_2 at temperatures above 380 °C.[55] According to the results obtained in the TPR analyses (Figure 2), it can be proposed that MoO_2 is the prevalent phase in this catalyst at the experimental activation and reaction conditions used in this work.[54]

On the other hand, the water content of the AP varied between 84.5 and 91.7 wt %, and the AP generated by pyrolysis without any catalytic treatment of the hot pyrolysis vapors had the greatest water content (Table 5). Therefore, the use of catalysts reduced the water content of the AP. High water contents in the liquid product collected resulted in AP liquids having a very low heating value, which restricts their use as fuel. In consequence, focus must be put on obtaining valuable chemicals from the AP.

Moreover, the small organic fraction present in the AP was rich in oxygen-containing aliphatic compounds (chromatographic area percentage >75%) such as carboxylic acids (mainly acetic acid), ketones, and alcohols (Figure 5). This, together with the presence of N-containing aliphatic compounds, resulted in this chemical family being prevalent amidst all the different identified compounds. Oxygen and/or nitrogen-containing aromatic compounds (both nonheterocyclic and heterocyclic) were also present (chromatographic area percentage between 9 and 20%). The most representative compounds of these two chemical families were phenol and pyridinol and their methyl derivatives, respectively.

In summary, the main chemical families were the same in both pyrolysis and pyrolysis, followed by downstream catalytic processing of the hot vapors. In general terms, the use of catalytic materials increased the proportion of oxygen- and/or nitrogen-containing heterocyclic aromatic compounds while decreasing the proportion of oxygen-containing aliphatic compounds and oxygen- and nitrogen-containing aliphatic compounds. Thus, the catalytic treatment of Amazonian cocoa pod husk pyrolysis hot vapors increased the degree of aromatization of the small organic fraction present in the AP. Interestingly, the bimetallic catalyst had a lesser impact on the AP composition, regardless of the way it was used (with or without preliminary activation). Therefore, the liquid product obtained in the runs carried out with $MoNi/Al_2O_3$ catalysts had an AP composition that resembled more that of bio-oil from pyrolysis without any catalytic treatment downstream. Since the predominant phases in the bimetallic MoNi catalysts, even after the ex situ reduction and passivation treatment, are MoO_3 and $NiMoO_4$ (see Figure 2, XRD analyses), it can be concluded that this material only shows certain hydrocracking activity when subjected to the activation treatment, which mainly affects the composition of the resulting OP and barely impacts the AP composition. The introduction of Mo in Ni/Al_2O_3 catalysts hinders the reduction of NiO, thus impacting negatively on the catalytic activity of Ni catalysts, though reduction of MoO_3 to MoO_2 is facilitated by the presence of NiO,[54] which could explain the results obtained.

Regarding the rest of the catalytic materials tested, similar AP compositions were obtained in all cases. The general relative increase in aromatic compounds detected in all their AP liquids, combined with the decrease detected in their corresponding OP. In catalytic pyrolysis, it is frequent the occurrence of deoxygenation, cracking, aromatization, and/or condensation reactions,[56] along with enhancing the conversion of pyrolysis intermediates of cellulose or hemicellulose to phenols caused by the presence of superheated water in pyrolysis volatiles, which reacts oxygen-containing functional groups, increasing acidity and promoting dehydration and decarbonization reactions.[57] Cracking reactions, for example, could provoke the cleavage and ring-opening of polycyclic aromatic compounds, thus yielding lighter organic compounds and fragments that may be redistributed between the two phases. In the absence of hydrogen, condensation routes are possible, leading to an increase in polyaromatic compounds and changes in chemical nature such as solubility in water, which could explain changes in product distribution. Comparisons with other studies in the literature are difficult since, to the best of our knowledge, most of the bio-oil upgrading processes use hydrogen in contrast to this contribution.

Again, the results obtained using standalone γ-Al_2O_3 as catalytic material help envision further bio-oil upgrading strategies, which could include the use of a preliminary

https://doi.org/10.1021/acsomega.3c06672
ACS Omega 2023, 8, 37610−37621

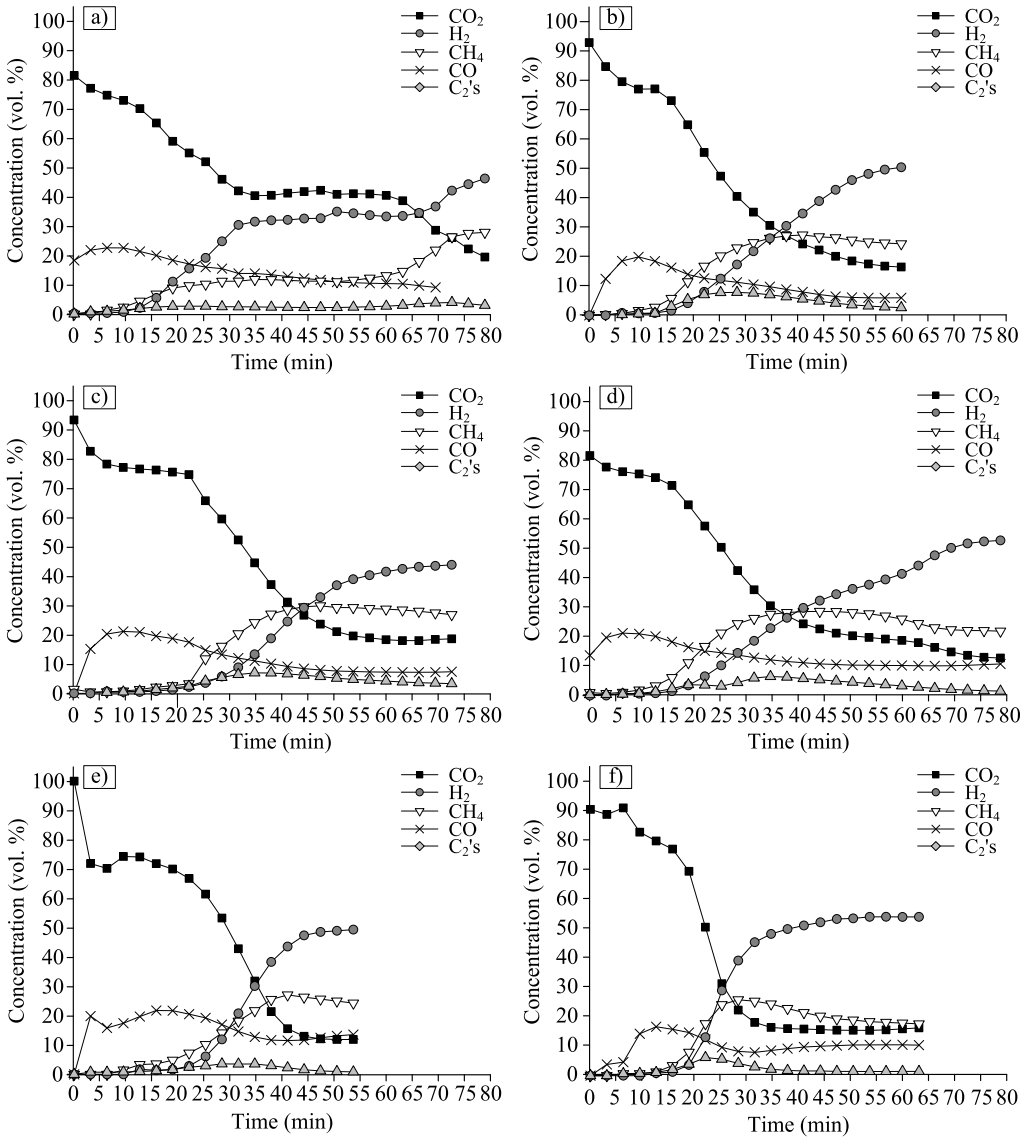

Figure 6. Evolution of permanent gases obtained from Amazonian cocoa pod husks pyrolysis and pyrolysis followed by downstream catalytic treatment of the hot vapors: (a) NC, (b) Al_2O_3, (c) Mo/Al_2O_3 RP, (d) Ni/Al_2O_3 RP, (e) $MoNi/Al_2O_3$ UR, and (f) $MoNi/Al_2O_3$ RP.

upgrading catalytic stage downstream from the pyrolysis reactor.

^{1}H and ^{13}C NMR measurements confirmed the presence of aromatic and aliphatic compounds both in the OP and the AP as concluded from GC−MS analysis, while HSQC-TOCSY provided additional insights about the composition of the OP showing similar cross-peaks in all cases which was related to methoxy groups (see the Supporting Information for more details). Moreover, HSQC-TOCSY crossed the peaks (Table S1) in the aromatic region confirmed the presence of phenolic, guaiacyl, and vanillin units in the samples which agrees with the O-containing aromatic fraction (Figure 4). Finally, DOSY-NMR measurements on the OP showed two significant diffusion traces in all samples, related to guaiacol and vanillin (Figure S5).[58−62]

3.2.3. Permanent Gases Analysis. Various reactions occur simultaneously along with devolatilization, including primary and secondary thermal cracking reactions, CO disproportionation (Boudouard equilibrium), steam reforming, and the water-gas-shift (WGS) equilibrium, among others, which is reflected in the evolution of the permanent gases' composition (Figure 6). Gas analyses were initiated once the desired pyrolysis temperature (500 °C) was reached. Anyhow, temperature gradients inside the pyrolysis reactor were somewhat expected, given the dimensions of the reactor and the limitations concerning heating rates that can be achieved with the electric furnace of the setup. Therefore, the induction period observed at the beginning of the runs (~15 min) can be explained by the occurrence of devolatilization of the most volatile species, which typically yield CO_2, CO, and steam as the main gaseous products. As the pyrolytic bed gradually increased its temperature, the release of volatiles occurred, and secondary thermal cracking reactions may explain the time evolution observed in the case of CH_4 and C_2's, which showed a noticeable uptake after the induction period.

When no catalytic treatment was applied to the hot pyrolysis vapors, the time evolution of both CH_4 and C_2's reached a plateau between *ca.* 15 and −55 min of reaction time. A similar trend was followed by H_2, though the plateau took place at longer reaction times (between 30 and 65 min approximately). This was likely caused by the massive release of volatiles and their evolution by secondary thermal cracking reactions into

https://doi.org/10.1021/acsomega.3c06672
ACS Omega 2023, 8, 37610−37621

smaller molecules. Next, there was another significant increase in the proportion of both CH_4 and H_2 together with a steady decay of CO_2 after approximately 60−65 min of reaction time, and a similar upward trend was observed by C_2 until *ca.* 72 min. However, the latter then showed a gradual decay until the end of the run. These results seemingly indicated that devolatilization has finished after 60 min of reaction. Later, solid carbonaceous residues may continue their thermal decomposition into more graphitized forms, which could result in the release of CH_4 and H_2, thus resulting in the release of CH_x species and, ultimately, H_2 by thermal cracking reactions of those species.

As for the different catalytic bed materials, similar trends were found in all cases. C_2's concentrations reached maxima at different reaction times for the different catalytic materials, showing different decays afterward. This, along with the steady asymptotic increase in H_2 production until the consecution of different maxima values of concentration in the product gases at the end of the runs, revealed that reforming reactions took place in the different catalytic beds.

If the time evolution of C_2's is carefully analyzed, the MoNi catalyst previously reduced and passivated (MoNi-RP) yielded a very fast abatement of C_2's once the maximum was reached, followed by the unreduced MoNi and closely followed by the monometallic catalysts. This may be explained by the activity for promoting reforming reactions of these catalysts along with the simultaneous occurrence of cracking reactions of different oxygenates in the volatile species and of different hydrocarbons both in the carbonaceous residues and in the volatiles, which is in accordance with NMR and GC−MS results showed above. The time evolution of CO_2 suggests that the WGS activity of the catalysts was low in any case, despite selecting a catalytic upgrading temperature that is thermodynamically favorable for promoting CO_2 and H_2 via the exothermic WGS reaction.

Regarding the CH_4 evolution over time in the different catalysts evaluated, the interpretation was difficult because the release of CH_4 due to progressive deactivation by coke deposition on the catalytic bed was combined with the partial reforming and cracking of the species on the surface of fresh catalyst particles downstream from the deactivation front.

It is also worth mentioning again the noticeable performance of bare γ-Al_2O_3 as a catalytic material. Cracking reactions can occur on the surface of this material, favored by its acidic nature, thus resulting in the decomposition of carbonaceous residues as well as other C-containing species into light hydrocarbons and hydrogen, which can explain the trends observed for CH_4, H_2, and C_2's contents in the product gas over the reaction time.

3.2.4. Spent Catalyst Characterization. Understanding the catalyst deactivation during the catalytic reaction is a key aspect to optimizing product distribution and operational process scale-up. Biomass is a challenging feedstock to process because a wide range of heteroatoms can lead to multiple issues than can affect the catalyst's lifetime. Some of the most relevant mechanisms for catalyst deactivation involved on biomass according to Santamaria et al.,[63] could be thermal, mechanical, or chemical nature.

On the one hand, thermal deactivation, normally linked to sintering issues, is caused when metal particles start to aggregate to form big metal particles (more stable configuration), leading to a reduction of active phase exposure. On the second one, the mechanical deactivation of catalysts is closely linked to fouling or attrition/crushing, which can easily rule out. Considering the reaction temperature leads to fluid adsorption in the catalyst pore or loss of activity due to material abrasion, which typically occurs on fluidized or circulating bed reactors. Finally, the chemical nature of the deactivation of catalysts involves poisoning, coke, and phase changes. The relevance of these three mechanisms depends on multiple factors, such as feedstock composition, catalyst, and reaction conditions. Generally, alumina has been the most widely used support in commercial Ni steam reforming catalysts[64,65] as its high specific surface area eases Ni dispersion, and its mechanical strength provides stability to the catalysts. However, the high rate of coke formation on catalysts based on alumina has been closely related to their acidity properties.

Based on the TPO analysis, it is possible to highlight that both, the reduced and passivated MoNi catalyst and the bare γ-Al_2O_3 bed had similar profiles which is indicative of similar coke characteristics (coke combustion temperature) lead by a lower amount of nickel and molybdenum incorporated on the support (Figure 7). The quantity of carbon deposited over the spent catalyst was calculated from the peak area, and both MoNi and bare γ-Al_2O_3 bed had similar deposited carbon amounts after the runs, 73 and 62 mg $C/g_{catalyst}$, respectively. A literature analysis about the nature of the coke formed in the reforming of bio-oil and pure oxygenates reactions over Ni nanoparticles, attributes these peaks to the combustion of three coke fractions: (i) an amorphous coke, encapsulating metal nanoparticles, and well-graphite nature.[66] In our case, MoNi (RP) showed a small shoulder at a higher temperature than the obtained for bare alumina, possibly associated with more graphitized or filament carbon lead by dehydrogenating reaction over Ni and Mo metals.

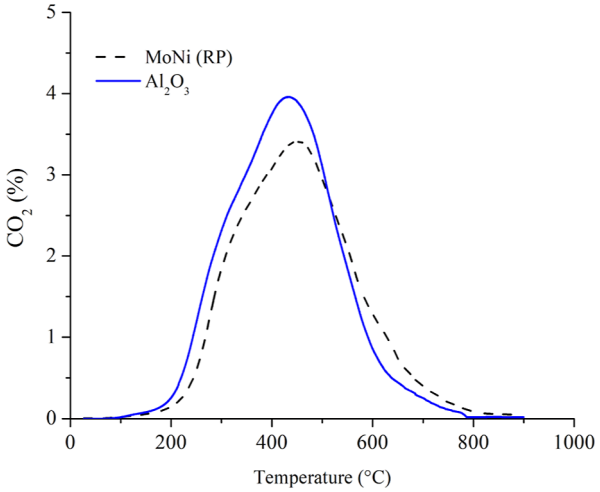

Figure 7. TPO profiles of spent MoNi catalysts and γ-Al_2O_3 (RP: reduced and passivated).

4. CONCLUSIONS

In this study, we proposed the valorization of one of Ecuador's major agricultural residues (Amazonian cocoa pod husks) with thermochemical processing by pyrolysis in the absence of hydrogen. Downstream catalytic processing of hot pyrolysis vapors using Mo- and/or Ni-based catalysts and standalone γ-Al_2O_3 was performed with the aim of enhancing the liquid

https://doi.org/10.1021/acsomega.3c06672
ACS Omega 2023, 8, 37610−37621

product properties and exploring chemical products composition.

Mo, Ni, and MoNi/γ-Al_2O_3 catalysts reduced the yield of the organic phase, but the homogeneity of the liquid product and the heating value remained constant. However, the use of catalytic materials increased the degree of aromatization of the small organic fraction present in the AP, revealed by the higher proportion of heterocyclic aromatic compounds containing O and/or N in contrast to the decrease of aliphatic homologues.

Pyrolysis gases were mainly composed of H_2, CO, CO_2, and light hydrocarbons. All catalytic reactions enriched the gaseous streams in CH_4, C_2's, and H_2 promoting reforming reactions along with cracking reactions of different oxygenate compounds, as confirmed by GC−MS results.

Pyrolysis of Amazonian cocoa pod husks can represent a potential improvement in the development of a biobased economy in Ecuador, bringing along numerous benefits and opportunities for the development of socially unfavored areas in the country by using biorefinery strategies to valorize agricultural residues. However, it is necessary to continue investigating the improvement of the liquid properties using catalysts and with different proofs of concept. In particular, the combination of a series of catalytic beds, including the use of standalone γ-Al_2O_3 as bulk inexpensive material as a preliminary catalytic bed, must be further explored in conjunction with further downstream catalytic processing of the pyrolysis vapors and/or collected liquid products.

■ ASSOCIATED CONTENT

Supporting Information

The Supporting Information is available free of charge at https://pubs.acs.org/doi/10.1021/acsomega.3c06672.

Catalyst characterization details, details of the GC- FID analysis, details on NMR sample preparation and analysis, additional details of catalysts properties, detailed discussion on thermogravimetric analysis of Amazonian cocoa pod husks, detailed discussion on NMR results, and additional figures and tables (PDF)

■ AUTHOR INFORMATION

Corresponding Author

Yanet Villasana − *Biomass Laboratory, Biomass to Resources Group, Universidad Regional Amazónica IKIAM, Tena 150150, Ecuador;* orcid.org/0000-0002-6677-5541; Email: yanet.villasana@kiam.edu.ec, ytvillas@gmail.com

Authors

Sabino Armenise − *Centro de Investigación Cepsa, Alcalá de Henares, Madrid 28805, Spain*

Javier Ábrego − *Grupo de Procesos Termoquímicos, Instituto Universitario de Investigación en Ingeniería de Aragón (I3A), Universidad de Zaragoza, Zaragoza 50018, Spain*

María Atienza-Martínez − *Grupo de Procesos Termoquímicos, Instituto Universitario de Investigación en Ingeniería de Aragón (I3A), Universidad de Zaragoza, Zaragoza 50018, Spain;* Present Address: Grupo de Reactores Químicos y Procesos para la Valorización de Recursos Renovables, Departamento de Ciencias, Edificio de los Acebos, Universidad Pública de Navarra, Campus de Arrosadía, E-31006 Pamplona, Spain

Karina Hablich − *Grupo de Reactores Químicos y Procesos para la Valorización de Recursos Renovables, Institute for Advanced Materials and Mathematics (InaMat2), Universidad Pública de Navarra (UPNA), Pamplona 31006, Spain*

Fernando Bimbela − *Grupo de Reactores Químicos y Procesos para la Valorización de Recursos Renovables, Institute for Advanced Materials and Mathematics (InaMat2), Universidad Pública de Navarra (UPNA), Pamplona 31006, Spain*

Alfonso Cornejo − *Grupo de Diseño, Síntesis Evaluación y Optimización de Nuevas Sustancias de Interés, Institute for Advanced Materials and Mathematics (InaMat2), Universidad Pública de Navarra (UPNA), Pamplona E-31006, Spain;* orcid.org/0000-0001-8810-0062

Luis M. Gandía − *Grupo de Reactores Químicos y Procesos para la Valorización de Recursos Renovables, Institute for Advanced Materials and Mathematics (InaMat2), Universidad Pública de Navarra (UPNA), Pamplona 31006, Spain;* orcid.org/0000-0002-3954-4609

Complete contact information is available at: https://pubs.acs.org/10.1021/acsomega.3c06672

Author Contributions

Conception and design of study: Yanet Villasana, Sabino Armenise, Javier Ábrego, and Fernando Bimbela. Acquisition of data: Yanet Villasana, Karina Hablich, Maria Atienza, and Sabino Armenise. Analysis and/or interpretation of data: Yanet Villasana, Fernando Bimbela, Sabino Armenise, Javier Ábrego, and Luis Gandía. Drafting the manuscript: Yanet Villasana, Sabino Armenise, Javier Ábrego, Fernando Bimbela, and Alfonso Cornejo. Revising the manuscript critically for important intellectual content: Yanet Villasana, Sabino Armenise, Javier Ábrego, Fernando Bimbela, and Luis Gandía. Approval of the version of the manuscript to be published: Yanet Villasana, Sabino Armenise, Javier Ábrego, Fernando Bimbela, Luis Gandía, Karina Hablich, and Maria Atienza.

Notes

The authors declare no competing financial interest.

■ ACKNOWLEDGMENTS

Authors would like to thank the Agencia Española de Cooperación Internacional para el Desarrollo (AECID) and Universidad Regional Amazónica Ikiam for the financial support provided to develop this contribution. The Spanish Ministerio de Ciencia, Innovación y Universidades and the European Regional Development Fund (ERDF/FEDER) are also thanked for providing financial support to the UPNA team (project ref. RTI2018-096294-B-C31). A.C. also thanks the Departamento de Desarrollo Económico del Gobierno de Navarra for the financial support in the "PC036-037 Biovalorización" Project. L.M.G. thanks Banco de Santander and Universidad Pública de Navarra for their financial support under "Programa de Intensificación de la Investigación 2018" initiative. The authors acknowledge the funding from the Aragón Government (ref. T22_17R), cofunded by FEDER 2014-2020 "Construyendo Europa desde Aragón". Authors would also like to acknowledge the use of Servicio General de Apoyo a la Investigación—SAI, Universidad de Zaragoza, and especially Dr. Concepción Sanchez for the XRD analyses and Dr. Ana Guitart and the rest of the team at the Servicio de Análisis Químico of the SAI for kindly conducting the ICP-OES analyses. K.H. thanks the Universidad Pública de Navarra for the predoctoral aid awarded by the UPNA to do her PhD

thesis. S.A. thanks Carlos Avila (Universidad Regional Amazónica Ikiam, Ecuador) and Diana Calero (Universidad Politécnica Salesiana, Ecuador) for inviting him to be part of their team during the past 5 years. Lastly, F.B. is also very grateful for the support and inspiration provided by David Sánchez and the rest of his group while developing this work.

REFERENCES

(1) Ministerio Coordinador de Producción, Empleo y Competitividad; Ministerio de Electricidad y Energía Renovable. *Atlas Bioenergético Del Ecuador*, 1st ed.; Quito, 2014.
(2) Voora, V.; Bermúdez, S.; Larrea, C. *Global Market Report: Cocoa*; International Institute for Sustainable Development, 2019; p 12.
(3) Agencia de Regulación y Control Fito y Zoosanitario, República del Ecuador. *Boletín Informativo: Informe Técnico de Exportación de Cacao*, 2022. https://www.agrocalidad.gob.ec/wp-content/uploads/2022/02/Informe-cacao.pdf.
(4) Adjin-Tetteh, M.; Asiedu, N.; Dodoo-Arhin, D.; Karam, A.; Amaniampong, P. N. Thermochemical Conversion and Characterization of Cocoa Pod Husks a Potential Agricultural Waste from Ghana. *Ind. Crops Prod.* **2018**, *119*, 304−312.
(5) Briens, C.; Piskorz, J.; Berruti, F. Biomass Valorization for Fuel and Chemicals Production - A Review. *Int. J. Chem. React. Eng.* **2008**, *6* (1), 1−49.
(6) Holladay, J. E.; White, J. F.; Bozell, J. J.; Johnson, D. *Top Value Added Chemicals from Biomass_lignin_Vol2.Pdf*, 2007; Vol. *II*.
(7) Jahirul, M. I.; Rasul, M. G.; Chowdhury, A. A.; Ashwath, N. Biofuels Production through Biomass Pyrolysis- A Technological Review. *Energies* **2012**, *5* (12), 4952−5001.
(8) Radlein, D.; Quignard, A. A Short Historical Review of Fast Pyrolysis of Biomass. *Oil Gas Sci. Technol.* **2013**, *68* (4), 765−783.
(9) Bimbela, F.; Oliva, M.; Ruiz, J.; García, L.; Arauzo, J. Steam Reforming of Bio-Oil Aqueous Fractions for Syngas Production and Energy. *Environ. Eng. Sci.* **2011**, *28* (11), 757−763.
(10) Bimbela, F.; Chen, D.; Ruiz, J.; García, L.; Arauzo, J. Ni/Al Coprecipitated Catalysts Modified with Magnesium and Copper for the Catalytic Steam Reforming of Model Compounds from Biomass Pyrolysis Liquids. *Appl. Catal., B* **2012**, *119*−*120*, 1−12.
(11) Bimbela, F.; Oliva, M.; Ruiz, J.; García, L.; Arauzo, J. Hydrogen Production via Catalytic Steam Reforming of the Aqueous Fraction of Bio-Oil Using Nickel-Based Coprecipitated Catalysts. *Int. J. Hydrogen Energy* **2013**, *38* (34), 14476−14487.
(12) García, L.; Ábrego, J.; Bimbela, F.; Sánchez, J. L. Hydrogen Production from Catalytic Biomass Pyrolysis. *Biofuels Biorefin.* **2015**, *5*, 119−147.
(13) Bimbela, F.; Ábrego, J.; Puerta, R.; García, L.; Arauzo, J. Catalytic Steam Reforming of the Aqueous Fraction of Bio-Oil Using Ni-Ce/Mg-Al Catalysts. *Appl. Catal., B* **2017**, *209*, 346−357.
(14) Gómez-Monedero, B.; Bimbela, F.; Arauzo, J.; Faria, J.; Ruiz, M. P. Pyrolysis of Red Eucalyptus, Camelina Straw, and Wheat Straw in an Ablative Reactor. *Energy Fuels* **2015**, *29* (3), 1766−1775.
(15) Chiaramonti, D.; Oasmaa, A.; Solantausta, Y. Power Generation Using Fast Pyrolysis Liquids from Biomass. *Renewable Sustainable Energy Rev.* **2007**, *11* (6), 1056−1086.
(16) Lehto, J.; Oasmaa, A.; Solantausta, Y.; Kytö, M.; Chiaramonti, D. Review of Fuel Oil Quality and Combustion of Fast Pyrolysis Bio-Oils from Lignocellulosic Biomass. *Appl. Energy* **2014**, *116*, 178−190.
(17) Li, D.; Li, X.; Gong, J. Catalytic Reforming of Oxygenates: State of the Art and Future Prospects. *Chem. Rev.* **2016**, *116* (19), 11529−11653.
(18) Dabros, T. M. H.; Stummann, M. Z.; Høj, M.; Jensen, P. A.; Grunwaldt, J.-D.; Gabrielsen, J.; Mortensen, P. M.; Jensen, A. D. Transportation Fuels from Biomass Fast Pyrolysis, Catalytic Hydrodeoxygenation, and Catalytic Fast Hydropyrolysis. *Prog. Energy Combust. Sci.* **2018**, *68*, 268−309.
(19) Zacher, A. H.; Olarte, M. V.; Santosa, D. M.; Elliott, D. C.; Jones, S. B. A Review and Perspective of Recent Bio-Oil Hydrotreating Research. *Green Chem.* **2014**, *16* (2), 491−515.
(20) Iisa, K.; Robichaud, D. J.; Watson, M. J.; ten Dam, J.; Dutta, A.; Mukarakate, C.; Kim, S.; Nimlos, M. R.; Baldwin, R. M. Improving Biomass Pyrolysis Economics by Integrating Vapor and Liquid Phase Upgrading. *Green Chem.* **2018**, *20* (3), 567−582.
(21) Imran, A.; Bramer, E. A.; Seshan, K.; Brem, G. An Overview of Catalysts in Biomass Pyrolysis for Production of Biofuels. *Biofuel Res. J.* **2018**, *5* (4), 872−885.
(22) Wang, D.; Zhu, Y.; Chen, J.; Li, W.; Luo, F.; Li, S.; Xie, W.; Liu, J.; Lan, H.; Zheng, Z. Catalytic Upgrading of Lignocellulosic Biomass Pyrolysis Vapors: Insights into Physicochemical Changes in ZSM-5. *J. Anal. Appl. Pyrolysis* **2021**, *156*, 105123.
(23) Liang, J.; Shan, G.; Sun, Y. Catalytic Fast Pyrolysis of Lignocellulosic Biomass: Critical Role of Zeolite Catalysts. *Renewable Sustainable Energy Rev.* **2021**, *139*, 110707.
(24) Imran, A.; Bramer, E. A.; Seshan, K.; Brem, G. High Quality Bio-Oil from Catalytic Flash Pyrolysis of Lignocellulosic Biomass over Alumina-Supported Sodium Carbonate. *Fuel Process. Technol.* **2014**, *127*, 72−79.
(25) Koike, N.; Hosokai, S.; Takagaki, A.; Nishimura, S.; Kikuchi, R.; Ebitani, K.; Suzuki, Y.; Oyama, S. T. Upgrading of Pyrolysis Bio-Oil Using Nickel Phosphide Catalysts. *J. Catal.* **2016**, *333*, 115−126.
(26) Iliopoulou, E. F.; Triantafyllidis, K. S.; Lappas, A. A. Overview of Catalytic Upgrading of Biomass Pyrolysis Vapors toward the Production of Fuels and High-Value Chemicals. *Wiley Interdiscip. Rev. Energy Environ.* **2019**, *8* (1), No. e322.
(27) Pucher, H.; Schwaiger, N.; Feiner, R.; Ellmaier, L.; Pucher, P.; Chernev, B. S.; Siebenhofer, M. Biofuels from Liquid Phase Pyrolysis Oil: A Two-Step Hydrodeoxygenation (HDO) Process. *Green Chem.* **2015**, *17* (2), 1291−1298.
(28) Stefanidis, S. D.; Kalogiannis, K. G.; Iliopoulou, E. F.; Lappas, A. A.; Pilavachi, P. A. In-Situ Upgrading of Biomass Pyrolysis Vapors: Catalyst Screening on a Fixed Bed Reactor. *Bioresour. Technol.* **2011**, *102* (17), 8261−8267.
(29) Mullins, D. R. The Surface Chemistry of Cerium Oxide. *Surf. Sci. Rep.* **2015**, *70* (1), 42−85.
(30) Horáček, J.; Kubička, D. Bio-Oil Hydrotreating over Conventional CoMo & NiMo Catalysts: The Role of Reaction Conditions and Additives. *Fuel* **2017**, *198*, 49−57.
(31) Izhar, S.; Uehara, S.; Yoshida, N.; Yamamoto, Y.; Morioka, T.; Nagai, M. Hydrodenitrogenation of Fast Pyrolysis Bio-Oil Derived from Sewage Sludge on NiMo/Al2O3 Sulfide Catalyst. *Fuel Process. Technol.* **2012**, *101*, 10−15.
(32) Pstrowska, K.; Walendziewski, J.; Łużny, R.; Stolarski, M. Hydroprocessing of Rapeseed Pyrolysis Bio-Oil over NiMo/Al2O3 Catalyst. *Catal. Today* **2014**, *223*, 54−65.
(33) Auersvald, M.; Shumeiko, B.; Staš, M.; Kubička, D.; Chudoba, J.; Simáček, P. Quantitative Study of Straw Bio-Oil Hydrodeoxygenation over a Sulfided NiMo Catalyst. *ACS Sustain. Chem. Eng.* **2019**, *7* (7), 7080−7093.
(34) Shetty, M.; Murugappan, K.; Prasomsri, T.; Green, W. H.; Roman-Leshkov, Y. Reactivity and Stability Investigation of Supported Molybdenum Oxide Catalysts for the Hydrodeoxygenation (HDO) of m-Cresol. *J. Catal.* **2015**, *331*, 86−97.
(35) Ranga, C.; Lødeng, R.; Alexiadis, V. I.; Rajkhowa, T.; Bjørkan, H.; Chytil, S.; Svenum, I. H.; Walmsley, J.; Detavernier, C.; Poelman, H.; et al. Effect of Composition and Preparation of Supported MoO3 Catalysts for Anisole Hydrodeoxygenation. *Chem. Eng. J.* **2018**, *335*, 120−132.
(36) Boullosa-Eiras, S.; Lødeng, R.; Bergem, H.; Stöcker, M.; Hannevold, L.; Blekkan, E. A. Catalytic Hydrodeoxygenation (HDO) of Phenol over Supported Molybdenum Carbide, Nitride, Phosphide and Oxide Catalysts. *Catal. Today* **2014**, *223*, 44−53.
(37) Murugappan, K.; Mukarakate, C.; Budhi, S.; Shetty, M.; Nimlos, M. R.; Román-Leshkov, Y. Supported Molybdenum Oxides as Effective Catalysts for the Catalytic Fast Pyrolysis of Lignocellulosic Biomass. *Green Chem.* **2016**, *18* (20), 5548−5557.
(38) Zhou, G.; Jensen, P. A.; Le, D. M.; Knudsen, N. O.; Jensen, A. D. Atmospheric Hydrodeoxygenation of Biomass Fast Pyrolysis Vapor by MoO3. *ACS Sustain. Chem. Eng.* **2016**, *4* (10), 5432−5440.

https://doi.org/10.1021/acsomega.3c06672
ACS Omega 2023, 8, 37610−37621

(39) Kukushkin, R. G.; Bulavchenko, O. A.; Kaichev, V. V.; Yakovlev, V. A. Influence of Mo on Catalytic Activity of Ni-Based Catalysts in Hydrodeoxygenation of Esters. *Appl. Catal., B* **2015**, *163*, 531−538.
(40) Moreira, R.; Moral, A.; Bimbela, F.; Portugal, A.; Ferreira, A.; Sanchez, J. L.; Gandía, L. M. Syngas Production via Catalytic Oxidative Steam Reforming of Glycerol Using a Co/Al Coprecipitated Catalyst and Different Bed Fillers. *Fuel Process. Technol.* **2019**, *189*, 120−133.
(41) Azuara, M.; Fonts, I.; Bimbela, F.; Murillo, M. B.; Gea, G. Catalytic Post-Treatment of the Vapors from Sewage Sludge Pyrolysis by Means of γ-Al2O3: Effect on the Liquid Product Properties. *Fuel Process. Technol.* **2015**, *130*, 252−262.
(42) Rogers, K. A.; Zheng, Y. Selective Deoxygenation of Biomass-Derived Bio-Oils within Hydrogen-Modest Environments: A Review and New Insights. *ChemSusChem* **2016**, *9*, 1750−1772.
(43) Jin, M.; Choi, M. Hydrothermal Deoxygenation of Triglycerides over Carbon-Supported Bimetallic PtRe Catalysts without an External Hydrogen Source. *Mol. Catal.* **2019**, *474*, 110419.
(44) Le Page, J.-F. *Catalyse de Contact: Conception, Préparation et Mise En Œuvre Des Catalyseurs Industriels*; Editions Technip, 1978.
(45) Plana, C.; Armenise, S.; Monzón, A.; García-Bordejé, E. Process Optimisation of In Situ H2 Generation From Ammonia Using Ni on Alumina Coated Cordierite Monoliths. *Top. Catal.* **2011**, *54* (13−15), 914−921.
(46) Ruiz-Gómez, N.; Quispe, V.; Ábrego, J.; Atienza-Martínez, M.; Murillo, M. B.; Gea, G. Co-Pyrolysis of Sewage Sludge and Manure. *Waste Manage.* **2017**, *59*, 211−221.
(47) Ábrego, J.; Plaza, D.; Luño, F.; Atienza-Martínez, M.; Gea, G. Pyrolysis of Cashew Nutshells: Characterization of Products and Energy Balance. *Energy* **2018**, *158*, 72−80.
(48) Channiwala, S. A.; Parikh, P. P. A Unified Correlation for Estimating HHV of Solid, Liquid and Gaseous Fuels. *Fuel* **2002**, *81* (8), 1051−1063.
(49) Trueba, M.; Trasatti, S. P. γ-Alumina as a Support for Catalysts: A Review of Fundamental Aspects. *Eur. J. Inorg. Chem.* **2005**, *2005* (17), 3393−3403.
(50) Yin, W.; Kloekhorst, A.; Venderbosch, R. H.; Bykova, M. V.; Khromova, S. A.; Yakovlev, V. A.; Heeres, H. J. Catalytic Hydrotreatment of Fast Pyrolysis Liquids in Batch and Continuous Set-Ups Using a Bimetallic Ni-Cu Catalyst with a High Metal Content. *Catal. Sci. Technol.* **2016**, *6* (15), 5899−5915.
(51) Henker, M.; Wendlandt, K.-P.; Valyon, J.; Bornmann, P. Structure of MoO3/Al2O3-SiO2 Catalysts. *Appl. Catal.* **1991**, *69* (1), 205−220.
(52) Arnoldy, P.; De Jonge, J. C. M.; Moulijn, J. A. Temperature-Programed Reduction of Molybdenum(VI) Oxide and Molybdenum-(IV) Oxide. *J. Phys. Chem.* **1985**, *89* (21), 4517−4526.
(53) Kordouli, E.; Kordulis, C.; Lycourghiotis, A.; Cole, R.; Vasudevan, P. T.; Pawelec, B.; Fierro, J. L. G. HDO Activity of Carbon-Supported Rh, Ni and Mo-Ni Catalysts. *Mol. Catal.* **2017**, *441*, 209−220.
(54) Borowiecki, T.; Gac, W.; Denis, A. Effects of Small MoO3 Additions on the Properties of Nickel Catalysts for the Steam Reforming of Hydrocarbons: III. Reduction of Ni-Mo/Al2O3 Catalysts. *Appl. Catal., A* **2004**, *270* (1−2), 27−36.
(55) Katrib, A.; Sobczak, J. W.; Krawczyk, M.; Zommer, L.; Benadda, A.; Jablonski, A.; Maire, G. Surface Studies and Catalytic Properties of the Bifunctional Bulk MoO2 System. *Surf. Interface Anal.* **2002**, *34* (1), 225−229.
(56) Ren, X.-Y.; Feng, X.-B.; Cao, J.-P.; Tang, W.; Wang, Z.-H.; Yang, Z.; Zhao, J.-P.; Zhang, L.-Y.; Wang, Y.-J.; Zhao, X.-Y. Catalytic Conversion of Coal and Biomass Volatiles: A Review. *Energy Fuels* **2020**, *34* (9), 10307−10363.
(57) Su, Y.; Liu, L.; Xu, D.; Du, H.; Xie, Y.; Xiong, Y.; Zhang, S. Syngas Production at Low Temperature via the Combination of Hydrothermal Pretreatment and Activated Carbon Catalyst along with Value-Added Utilization of Tar and Bio-Char. *Energy Convers. Manage.* **2020**, *205*, 112382.
(58) Li, D.; Kagan, G.; Hopson, R.; Williard, P. G. Formula Weight Prediction by Internal Reference Diffusion-Ordered NMR Spectroscopy (DOSY). *J. Am. Chem. Soc.* **2009**, *131* (15), 5627−5634.
(59) Ge, W.; Zhang, J. H.; Pedersen, C. M.; Zhao, T.; Yue, F.; Chen, C.; Wang, P.; Wang, Y.; Qiao, Y. DOSY NMR: A Versatile Analytical Chromatographic Tool for Lignocellulosic Biomass Conversion. *ACS Sustain. Chem. Eng.* **2016**, *4* (3), 1193−1200.
(60) Kuznetsov, B. N.; Chesnokov, N. V.; Sudakova, I. G.; Garyntseva, N. V.; Kuznetsova, S. A.; Malyar, Y. N.; Yakovlev, V. A.; Djakovitch, L. Green Catalytic Processing of Native and Organosolv Lignins. *Catal. Today* **2018**, *309* (December 2017), 18−30.
(61) Rencoret, J.; Marques, G.; Gutiérrez, A.; Nieto, L.; Santos, J. I.; Jiménez-Barbero, J.; Martínez, Á. T.; del Río, J. C. HSQC-NMR analysis of lignin in woody (*Eucalyptus globulus* and *Picea abies*) and non-woody (*Agave sisalana*) ball-milled plant materials at the gel state 10th EWLP, Stockholm, Sweden, August 25−28, 2008. *Holzforschung* **2009**, *63* (6), 691−698.
(62) Wen, J. L.; Sun, S. L.; Yuan, T. Q.; Xu, F.; Sun, R. C. Structural Elucidation of Lignin Polymers of Eucalyptus Chips during Organosolv Pretreatment and Extended Delignification. *J. Agric. Food Chem.* **2013**, *61* (46), 11067−11075.
(63) Santamaria, L.; Lopez, G.; Arregi, A.; Amutio, M.; Artetxe, M.; Bilbao, J.; Olazar, M. Stability of Different Ni Supported Catalysts in the In-Line Steam Reforming of Biomass Fast Pyrolysis Volatiles. *Appl. Catal., B* **2019**, *242*, 109−120.
(64) Arregi, A.; Lopez, G.; Amutio, M.; Barbarias, I.; Santamaria, L.; Bilbao, J.; Olazar, M. Regenerability of a Ni Catalyst in the Catalytic Steam Reforming of Biomass Pyrolysis Volatiles. *J. Ind. Eng. Chem.* **2018**, *68*, 69−78.
(65) Meloni, E.; Martino, M.; Palma, V. A Short Review on Ni Based Catalysts and Related Engineering Issues for Methane Steam Reforming. *Catalysts* **2020**, *10*, 352.
(66) Fakeeha, A. H.; Kasim, S. O.; Ibrahim, A. A.; Abasaeed, A. E.; Al-Fatesh, A. S. Influence of Nature Support on Methane and CO2 Conversion in a Dry Reforming Reaction over Nickel-Supported Catalysts. *Materials* **2019**, *12*, 1777.

https://doi.org/10.1021/acsomega.3c06672
ACS Omega 2023, 8, 37610−37621